CHEMISTRY
A EUROPEAN JOURNAL

DOI: 10.1002/chem.200500482

A Theoretical Investigation into the Photophysical Properties of Ruthenium Polypyridine-Type Complexes

Marie-France Charlot,*[a] Yann Pellegrin,[a] Annamaria Quaranta,[b, c] Winfried Leibl,[b] and Ally Aukauloo[a]

Abstract: Excited states of ruthenium polypyridine-type complexes have always attracted the interest of chemists. We have recently found evidence of a remarkable long-lived excited state (30 μs) for a Ru^{II} complex containing a heteroditopic ligand that can be viewed as a fused phenanthroline and salophen ligand.[1] To unravel this intriguing electronic property, we have used density functional theory (DFT) calculations to understand the ground-state properties of $[(bpy)_2Ru(LH_2)]^{2+}$, where LH_2 represents *N*,*N*′-bis(salicylidene)-(1,10-phenanthroline)diamine. Excited singlet and triplet states have been examined by the time-dependent DFT (TDDFT) formalism and the theoretical findings have been compared with those for the parent complex $[Ru(bpy)_3]^{2+}$. The outstanding result is the presence of excited states lower in energy than the metal-to-ligand charge-transfer states, originating from intraligand charge transfer (ILCT) from the phenolic rings to the phenanthroline part of the coordinated LH_2. The spin density distribution for the lowest triplet state provides evidence that it is in fact the lowest triplet state of the free ligand. Correlation between the energy level diagram of orbitals for the ground state and that for the ^{3}ILCT state clearly establishes that the ruthenium retains its formal Ru^{II} oxidation state. The quenching of the luminescence and the evidence of the long-lived excited state observed for $[(bpy)_2Ru(LH_2)]^{2+}$ are discussed in the light of the computational results.

Keywords: density functional calculations · electronic properties · excited states · photophysical processes · ruthenium

Introduction

Ruthenium(II) polypyridine-type complexes are archetypal complexes in the study of photoinduced electron or energy transfer.[2] The prominent electronic feature in the behaviour of such complexes stems from a unique combination of their ground state redox reactivity and excited state properties. Since the discovery that, upon irradiation with visible light, the long-lived excited state of $[Ru(bpy)_3]^{2+}$ can be either oxidised[3] or reduced in subsequent bimolecular reactions, a cornucopia of papers reporting the potential applications of this unique property has appeared in the literature.[4] More recently, the parent $[Ru(bpy)_3]^{2+}$ compound has found use as the photoactive component in the design of supramolecular systems with the aim of elaborating novel photocatalysts.[5–8] One such model compound can be seen as a $[Ru(bpy)_3]^{2+}$ core connected to a coordination metal complex capable of driving an interesting chemical reaction, be it an oxidation or a reductive process. The objectives behind the construction of such systems are numerous. In one, the diffusional limits between the donor and acceptor are eliminated. Another important parameter, the intramolecular separation between the integrative parts, can easily be modulated by synthetic procedures. The chemical nature of the bridging ligand may play a significant role in the photophysical properties and electron trade of the whole system. Hence, in the assemblage of these modular molecular units, successful progress towards a functioning model may rely on the photophysical behaviour of the lumophore.

[a] Dr. M.-F. Charlot, Dr. Y. Pellegrin, Prof. A. Aukauloo
Laboratoire de Chimie Inorganique, UMR 8613
Université de Paris-Sud
91405 Orsay (France)
Fax: (+33) 1 69154754
E-mail: mcharlot@icmo.u-psud.fr

[b] Dr. A. Quaranta, Dr. W. Leibl
Service de Bioénergétique
CEA Saclay, Bât. 532
91191 Gif-sur-Yvette Cedex (France)

[c] Dr. A. Quaranta
Muséum National d'Histoire Naturelle
Laboratoire de Chimie et de Biochimie des Substances Naturelles
UMR 5154 CNRS/USM 0502 CNRS
63 rue Buffon, 75005 Paris (France)

It is therefore of paramount importance to understand the intimate nature of the ground and excited states of the different photoactive building blocks.

While the properties of the ground and excited states of d^6 polypyridine complexes—$[Ru(bpy)_3]^{2+}$, for instance—have been investigated by a large variety of experimental techniques, computational studies remain scarce. The understanding of the photochemistry of transition metal complexes is still a great challenge to the interplay between calculation and experiment, because it requires good descriptions both of the ground state and of the appropriate excited states. However, theoretical analysis of the electronic states of these complexes faces major difficulties, in the shape of the large size of the molecules and the presence of strong electronic correlations. Quantum-mechanical methods based on the Hartree–Fock theory need post-Hartree–Fock treatments to provide reliable descriptions of the excited states,[9] but such approaches rapidly become intractable as the size of the system increases. This explains why calculations have until recently been performed with semiempirical methods[10,11] or on small models of the studied complex. In contrast, density functional theory (DFT) has been successful in the study of the ground-state properties of large transition-metal complexes. This is particularly true when a hybrid functional—such as B3LYP[12]—including a mixture of Hartree–Fock exchange with DFT exchange-correlation is used. In the case of ruthenium compounds, the influence of diimine-type ligands has been investigated to interpret photonic[13] or electrochemical properties,[14] as well as the ability to interact with DNA.[15,16] More recently, time-dependent density functional theory (TDDFT)[17] has proven its aptitude for calculation of the vertical electronic excitation energies responsible for the absorption spectra of Ru^{II} complexes.[18–20] The solvatochromism phenomenon has even been evaluated for some systems.[20] For small complexes such as $[Ru(NH_3)_4(bpy)]^{2+}$, Lever et al.[10,21] have compared different methods—semiempirical INDO/S methods and TDDFT performed with different functionals and basis sets—used for the calculation of electronic spectra. They concluded that the B3LYP functional usually gives the best results both for geometry optimisations and for electronic spectra.

The interpretation of photophysical properties introduces a further step of difficulty into the computation because, starting from a singlet ground state, triplets states are now involved. A DFT approach was first proposed by Daul et al.[22] Recently published TDDFT results have concerned complexes of Re^{I},[23] Ru^{II}[11] and Ir^{III}.[24]

We have recently reported[1] the synthesis and characterisation of the heteroditopic ligand *N*,*N*′-bis(3,5-di-*tert*-butylsalicylidene)-5,6-(1,10-phenanthroline)diamine, which can be viewed as a fused phenanthroline and a tetradentate Schiff base cavity. The properties—including electrochemistry, UV/Vis spectroscopy and photophysical studies—of the related complex derived from $[Ru(bpy)_3]^{2+}$ by substitution of one bpy by the ligand have been described. A rapid quenching of the emission was observed and a remarkable long-lived (30 μs) excited state was detected. Comments by the referees of this work encouraged us to analyse this state more profoundly, and so the ultimate goal of this work is to interpret this notable behaviour in the light of a theoretical approach, and in this paper we therefore investigate the structures and electronic properties of the ground state and lowest singlet and triplet excited states of a complex $[(bpy)_2Ru(LH_2)]^{2+}$ (abbreviated as **Ru-L**), in which LH_2 represents the unsubstituted derivative of the above ligand. We have also analysed the properties of the parent $[Ru(bpy)_3]^{2+}$ molecule (abbreviated as **Ru-bp**) by the same procedure, both to test the computational method and to derive comparisons between the two complexes.

Results

After a description of the computational methods that we have used, the Theoretical Results section is then composed of five parts:

1) The calculated optimised molecular structures are described for the free ligand and for the **Ru-L** complex. Reference is also made to our calculated values for **Ru-bp**.
2) The energy level diagrams for the ground states of the ligand and the **Ru-L** complex are presented and the frontier molecular orbitals are depicted. Correlations are established between the MOs of the free and the coordinated ligand.
3) The first excited states for both **Ru-L** and **Ru-bp** are calculated in this part by use of the optimised geometry of the ground state. We report their energies and their character emanating from electron promotion from occupied ground state MOs to vacant ones. Excited singlet and triplet states are considered separately.
4) The lowest triplets states of **Ru-bp** and **Ru-L** are considered in their own optimised geometries. The energy level diagram of the triplet spin-orbitals are described and correlation is made with the ground state molecular orbitals. The natures of these states are discussed.
5) Finally, the oxidised complexes are examined. This last section is devoted to the interpretation of some photophysical properties of **Ru-L** and **Ru-bp** in the light of our calculations, and is followed by a discussion of the relevance of the results.

Computation methods

Density functional theory calculations were carried out by use of Becke's three-parameter hybrid functional B3LYP[12] including Becke's gradient correction[25] for the exchange functional, along with nonlocal terms derived by Lee, Yang and Parr[26] for the correlation functional. The LanL2DZ basis set was employed. This consists of Dunning and Huzinaga's valence double-ζ basis D95V[27] for first row atoms and the Los Alamos effective core potential (ECP)[28] in-

cluding relativistic effects plus double-ζ atomic orbitals for heavier atoms. As no X-ray data are available either for the ligand or for the **Ru-L** complex, all geometries were fully optimised in the ground state (closed-shell singlet S_0). However, to decrease the computation time, the *tert*-butyl (*t*Bu) groups on the phenol rings were suppressed and a C_2 symmetry was retained. Test calculations on the free ligand with four *t*Bu groups or with C_1 symmetry have shown that the nature and energy ordering of the frontier orbitals are only slightly affected.

Starting from the closed-shell S_0 state, time-dependent density functional (TDDFT)[17] calculations were performed with a spin-restricted formalism to determine the energies and character of the lowest excited singlet and triplet states at the ground-state geometry.

In a different approach, spin-unrestricted calculations were employed to investigate the first spin–triplet state T_1 for the ligand LH_2, and also for the **Ru-L** and **Ru-bp** complexes, more completely. The corresponding geometries were fully optimised at the UB3LYP/LanL2DZ level of theory and the nature of these states were ascertained by analysis of the triplet spin-orbitals and of the spin density distribution. Furthermore, we have also performed similar calculations on $[Ru(bpy)_3]^{2+}$ in D_3 symmetry to underpin our theoretical data relating to $[(bpy)_2Ru(LH_2)]^{2+}$.

All calculations were carried out with the Gaussian 98 software package.[29]

Theoretical results

As mentioned earlier, we have studied the *N*,*N*′-bis(3,5-di-*tert*-butylsalicylidene)-5,6-(1,10-phenanthroline)diamine ligand experimentally (Figure 1, left), but our computation studies concern the simplified ligand, in which the two *tert*-butyl groups on each phenol ring have been suppressed. The structure of the complex $[(bpy)_2Ru(LH_2)]^{2+}$ is also reported in the same figure, as it is the result of geometry optimisation calculations.

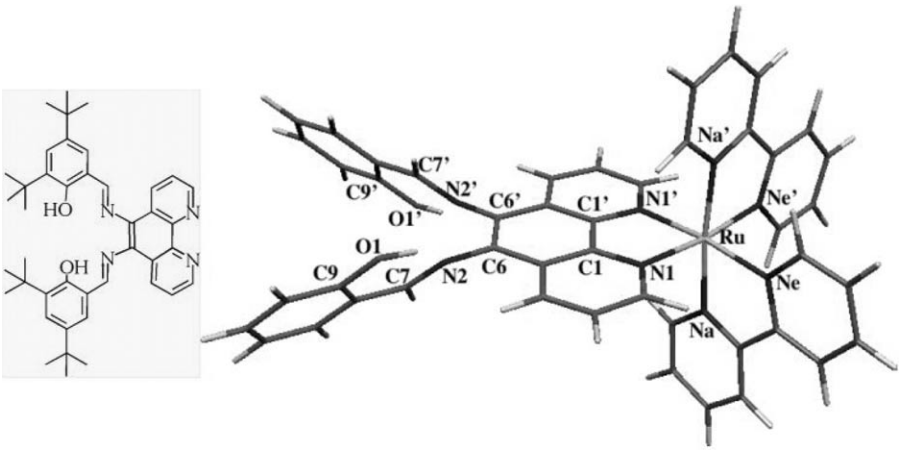

Figure 1. Free ligand LH_2 (left) and the calculated structure of the complex $[(bpy)_2Ru(LH_2)]^{2+}$ (right), with numbering of the atoms.

Molecular structures: Selected optimised geometric parameters calculated for the ground state S_0 and the lowest triplet state T_1 of the ligand and the ruthenium complexes are reported in Table 1.

Free ligand: The computed structure of the ligand in the S_0 ground state was described in the previous paper. Steric hindrance between the protons on C3 and C7 (and C3′/C7′) induces a distortion. In the singlet state, the two nitrogen atoms N2 and N2′ stay in the plane defined by the phenanthroline skeleton, while torsion of the pending phenol groups occurs mainly around the C6–N2 and C6′–N2′ bonds (see dihedral angle C6′-C6-N2-C7). It may be noted that the salophen N_2O_2 cavity is not planar in the absence of a coordinating metal ion. In the lowest triplet state a more drastic molecular distortion arises: the phenanthroline skeleton no longer remains planar overall and the two nitrogen atoms N2 and N2′ depart from its mean plane, as indicated by the value (40.9°) of the dihedral angle N2′-C6′-C6-N2. The major torsion occurs around the C6–C6′ bond of phenanthroline and, to a lesser extent, around C6–N2 and C6′–N2′. Another remarkable change on going from the singlet to the triplet state is the variation in the bond lengths in the C6′-C6-N2-C7 fragment (and in the symmetric one). Actually, we noticed that a lengthening of the central C6–N2 bond occurs, while the two outer C6′–C6 and N2–C7 bonds are shortened. These geometric modifications denote an important change in conjugation between the two states (S_0 and T_1, respectively), in this part of the molecule. Hence, the conclusive point to recall from our calculations for the $S_0 \rightarrow T_1$ pathway of the ligand is the substantial geometric change.

Complex: In the computed structure of the **Ru-L** complex, the ruthenium(II) adopts, as usual, a distorted octahedral coordination geometry. The geometry of the ligand LH_2 remains essentially unchanged on going from the free ligand to the complex in the ground state. The main change is the small shrinkage of the C1–C1′ bond in both S_0 and T_1 states, as a consequence of the coordination to ruthenium. The relatively poor quality of the basis set (valence double-ζ) and the large size of the system, which makes the geometry optimisations complicated, prevent us from taking minor changes in the metric parameters into consideration. All Ru–N bond lengths are in almost the same range (2.10 Å, as also calculated for $[Ru(bpy)_3]^{2+}$) and so we do not take account of these small and meaningless differences in this paper.

Table 1. Selected calculated geometric parameters for ligand LH_2, complex $[(bpy)_2Ru(LH_2)]^{2+}$ and $[Ru(bpy)_3]^{2+}$ in their ground singlet states S_0 and in their first excited triplet states T_1. Values for the oxidised complex $[(bpy)_2Ru(LH_2)]^{3+}$ are also reported.

	LH_2		$[(bpy)_2Ru(LH_2)]^{2+}$			$[Ru\ bpy)_3]^{2+}$	
	S_0	T_1	S_0	T_1	ox[a]	S_0	T_1
			distances [Å]				
Ru−N1			2.109	2.104	2.107		
Ru−Na			2.097	2.096	2.104	2.100	2.093
Ru−Ne			2.095	2.098	2.101	2.100	2.093
C1−C1′	1.463	1.489	1.432	1.455			
C6−C6′	1.391	1.491	1.406	1.492			
C6−N2	1.424	1.351	1.408	1.366			
N2−C7	1.314	1.360	1.323	1.357			
C9−O1	1.371	1.371	1.373	1.367			
			angles [°]				
N1-Ru-N1′			79.3	78.9			
N1-Ru-Na			88.3	88.4			
N1-Ru-Ne			95.8	96.2			
N1-Ru-Na′			96.4	96.4			
Na-Ru-Ne			78.5	78.5		78.4	78.9
Na-Ru-Ne′			97.2	97.0		96.7	97.2
Ne-Ru-Ne′			89.5	89.1		88.4	87.1
C6′-C6-N2	123.2	124.3	124.2	124.3			
C6-N2-C7	122.8	125.6	124.4	126.0			
N2-C7-C8	121.3	120.6	121.7	121.0			
			dihedral angles [°]				
N2′-C6′-C6-N2	−1.3	40.9	−4.9	31.2	1.6		
C6′-C6-N2-C7	57.6	10.9	55.3	17.1	49.1		
C6-N2-C7-C8	−179.4	−176.7	−178.1	−175.0	−177.7		

[a] Oxidised complex.

Energy levels and molecular orbitals in the ground state

Orbitals of the ligand: In a previous study of the ligand only, we depicted its molecular orbitals and discussed its bichromophoric character. The frontier orbitals can be classified as being more predominantly developed either on the phenanthroline moiety or on the salophen skeleton. The LUMO and LUMO+1 consist predominantly of the *a*- and *b*-symmetry combinations of the antibonding π* orbitals of the C=N imino groups, with no contribution on the phenanthroline extremity. However, the LUMO+2 and LUMO+3 are essentially the π* (locally *b1* ψ) and (locally *a2* χ) orbitals of phenanthroline (see, for instance, reference [30] for reference to ψ and χ). In contrast, the HOMO of *b* symmetry is developed on the whole ligand, with an important electronic distribution in the C1−C1′ bond. As we will see further, two other occupied orbitals will play an important part in the complex; these are the HOMO−1 and HOMO−3, which are the *a* and *b* combinations, respectively, of the orbitals located on the two symmetric phenol groups. The HOMO−2 and HOMO−4 are the two σ orbitals spread on the nitrogen atoms of the phenanthroline end, with *b* and *a* symmetry, respectively, and are responsible for the coordination to ruthenium in the complex. We must stress the fact that they are not the highest occupied orbitals, as is usually the case for polypyridine ligands without oxygenated substituents. Furthermore, it is interesting to notice that the calculated HOMO–LUMO gap is 3.58 eV, which is notably smaller than the value of 4.61 eV that we have determined for phenanthroline by the same method.

Orbitals of the $[(bpy)_2Ru(LH_2)]^{2+}$ complex: In a logical way, we now examine the highest occupied and lowest virtual orbitals for the **Ru-L** complex in its S_0 singlet ground state (state ^1A in C_2 symmetry). As will be seen later, these MOs provide the framework for the excited state description by TDDFT. Their energies and characters govern the absorption and emission spectra to a large extent, as well as the nature of the transitions. The symmetries, energies and preponderant compositions of these orbitals are listed in Table 2.

The assignment of the type of each MO is the result of visual inspection of its three-dimensional representation (see Figure 2). The energy diagram (in atomic units) of the frontier

Table 2. Calculated frontier orbitals of $[(bpy)_2Ru(LH_2)]^{2+}$ in the ground singlet state (S_0): symmetry in the C_2 group, energy in atomic units [a.u.] and dominant character.

Orbital	Symmetry	Energy [a.u.]	Dominant character[a]
occupied			
188	*a*	−0.448	π(phen) + π(bpy)
189	*b*	−0.447	π(bpy)
190	*a*	−0.427	salophen
191	*b*	−0.406	salophen
192	*a*	−0.401	d_π(Ru)
193	*b*	−0.399	d_π(Ru)
194	*a*	−0.395	d_π(Ru)
195	*a*	−0.394	salophen
196	*b*	−0.377	C1=C1′(phen) + PhOH
197	*a*	−0.362	PhOH
198	*b*	−0.358	PhOH
virtual			
199	*b*	−0.272	π_1*(bpy)
200	*a*	−0.269	π_1*(bpy)
201	*b*	−0.261	ψ(phen)
202	*a*	−0.256	χ(phen)
203	*b*	−0.242	π_2*, π_3*(bpy)
204	*a*	−0.234	π_2*, π_3*(bpy)
205	*a*	−0.231	π_2*, π_3*(bpy)
206	*b*	−0.231	π_2*, π_3*(bpy)
207	*b*	−0.220	C7=N2 + π*(phen)
208	*a*	−0.216	C7=N2 + π*(phen)

[a] π(phen) and π(bpy): highest π occupied orbitals of the free ligands. π_1*(bpy), π_2*(bpy), π_3*(bpy): unoccupied orbitals of bipyridine in increasing order. χ(phen) and ψ(phen): the two π* LUMOs of phenanthroline of *a* and *b* symmetry, respectively. PhOH: orbitals on the phenol rings of LH_2. salophen: orbitals developed on the salophen cavity. C1=C1′(phen): see Figure 1. C7=N2 (and C7′=N2′): imine groups of the salophen.

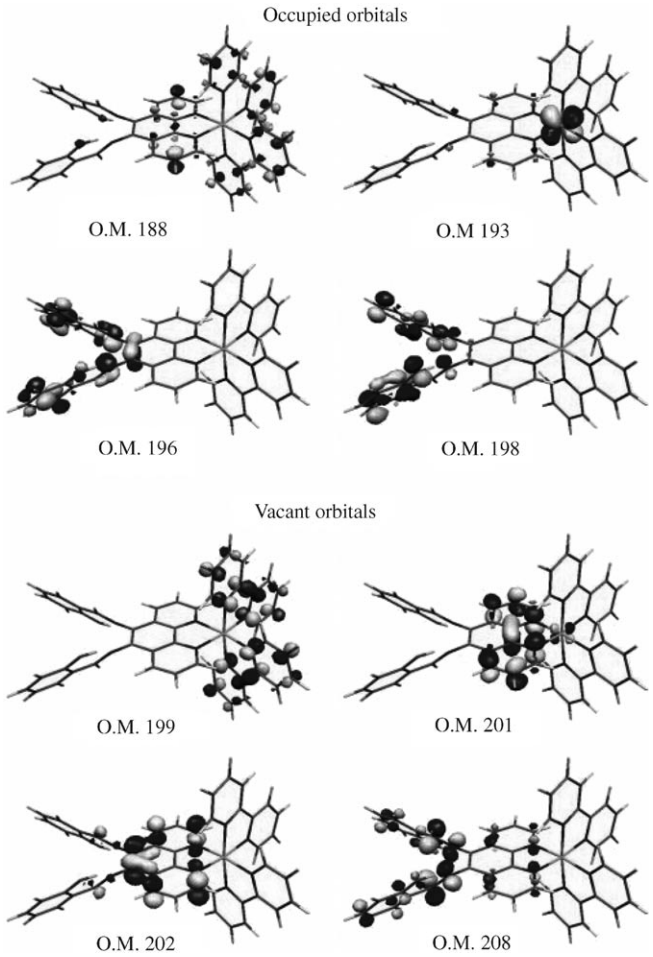

Figure 2. Selected orbitals of $[(bpy)_2Ru(LH_2)]^{2+}$ in its ground state.

orbitals of **Ru-L** is plotted in Figure 3, and a correlation is established between these MOs and the orbitals of the building bpy and LH_2 ligands. The analogous correspondence between the orbitals of $[Ru(bpy)_3]^{2+}$ (state $^1A_1$ in D_3 symmetry) and of bpy is also shown in Figure 3 for discussion.

However, direct energy comparison between molecules bearing different total charges is not relevant, because the gain in stability produced by the electron–nucleus attractive potential stabilises the total energy of a molecule more and more while its positive charge increases. As we noticed that the first vacant orbital (π_1*) of the bipyridine ligand remains almost unchanged in the first set of unoccupied orbitals (LUMO and LUMO+1 for **Ru-L** and LUMO to LUMO+2 for **Ru-bp**), we used a mathematical artifice to allow easier reading of the correspondences between the energy level diagrams: we shifted all the energies for both complexes in such a way as to level the energies for all MOs corresponding to π_1* orbitals. This is achieved by adding 0.210 a.u. to all energies for **Ru-L** and 0.215 a.u. for **Ru-bp** (see Figure 3).

As can be seen in Figure 3 and Table 2, the highest occupied orbitals of **Ru-L** are not ruthenium d_π orbitals as in **Ru-bp** but ligand-centred orbitals. From our preliminary calculations, this occurs because the ligand possesses occupied orbitals higher in energy than the σ orbitals susceptible to coordination to the ruthenium ion. In **Ru-L**, HOMO (198) and HOMO−1 are, in the order given, the *b* and *a* combinations of orbitals developed over the whole phenol rings; they are strongly reminiscent of HOMO−3 and HOMO−1, respectively, of LH_2. This point is consistent with the first anodic electron transfer observed by cyclic voltammetry, which can be attributed to the removal of one electron from the phenol group. The next occupied orbital in decreasing order (i.e., 196) is derived from the HOMO of the ligand developed on C6=C6′ and on the whole Schiff base; a small contribution on the phen end of the ligand is responsible for a stabilisation, greater than that for the phenolic orbitals, upon coordination to the ruthenium. Orbital 195 develops on the salophen (but not on the phenolic oxygen atoms). The next three orbitals (194–192) are nearly pure d_π orbitals of ruthenium(II), and the two following ones are located on the LH_2 ligand. Finally, MOs 189 and 188 are occupied π orbitals on bpy and phen + bpy, respectively.

We now consider the vacant orbitals in increasing order. The first ones (199, 200) are the *b* and *a* combinations, respectively, of the π_1* orbitals of the two bipyridines. The next two are the well known vacant π* orbitals of the phenanthroline part: ψ (*b*) and χ (*a*). Orbitals 203 to 206 are combinations of the π_2* and π_3* orbitals resulting from small ligand–ligand interactions. Finally, MOs 207 (*b*) and 208 (*a*) are essentially located on the imine parts (C7=N2 and C7′=N2′) of the main ligand. They issue from the two LUMOs of the free ligand LH_2 but are strongly destabilised and now mix with high-lying π* orbitals of phenanthroline.

A telling fact from the diagram in Figure 3 is that the HOMO–LUMO energy gap is quite a lot smaller in **Ru-L** (2.34 eV) than in **Ru-bp** (3.36 eV). In contrast, the mean difference in energy between the set of d_π orbitals and the set of π_1*(bpy) orbitals is nearly the same: 3.49 eV for **Ru-L** and 3.56 eV for **Ru-bp**. It is not surprising that the excitation energies, discussed later, reflect the comparison of these gaps, with Ru to bpy charge transfers at nearly the same energy in both complexes and a spectrum expanding more in the near infrared region for **Ru-L** than for **Ru-bp.**

Excited states: TDDFT calculations were employed to examine the low-lying singlet and triplet excited states of the **Ru-L** complex, as well as those of **Ru-bp**, in their ground-state geometries. This means that vertical excitation energies from the ground state are calculated. Excited states' electronic structures are described in terms of multiconfigurations: that is, a linear combination of several occupied to virtual MO (or spin–orbital) excitations comprises a given electronic transition. Consequently, the dominant character of each transition can be clearly specified. TDDFT also provides the electric dipole oscillator strength (*f*) of the transition from the ground to the excited state, which is related to the transition moment, thereby allowing the description of the electronic spectrum of the molecule (in the gas phase).

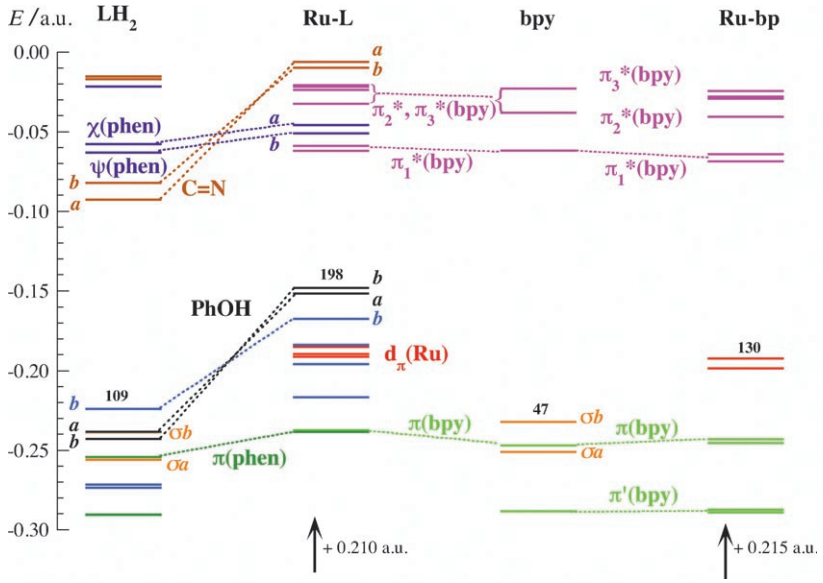

Figure 3. Energy level diagram (in atomic units: a.u.) of frontier MOs for $[(bpy)_2Ru(LH_2)]^{2+}$ in its ground state and correlation with the orbitals of the constituent ligands (LH_2) and (bpy). A similar correlation for $[Ru(bpy)_3]^{2+}$ is presented on the right-hand side. The energy levels for **Ru-L** and **Ru-bp** are shifted by 0.210 and 0.215 a.u., respectively, to allow for the +2 charge of the complexes as compared to the 0 charge of the ligands (see text).

As spin–orbit effects are neglected in current TDDFT calculations, transitions from the ground state to the triplet states are spin-forbidden and the *f* values for transitions from S_0 to these states are all zero.

For the singlet states, selected transitions with noticeable *f*-values (except the first one) are reported in Table 3, whilst the results for all lowest triplets are displayed in Table 4.

Excited singlet states: A full description of the UV/Vis spectrum of the complex by DFT calculations lies beyond the scope of this study. Accordingly, high-energy excited singlet states responsible for the ultraviolet part of the absorption spectrum have not been investigated. Indeed, their study is highly time-consuming, especially in large systems with low symmetry. Furthermore, they are responsible for $\pi\rightarrow\pi^*$ transitions, which do not participate in the photophysics of ruthenium complexes. In fact, 45 states describing transitions above 360 nm have been calculated, but nonetheless no transition originating from π orbitals, either from bipyridine or from phenanthroline, was found.

Looking at Table 3, we notice that the lowest states ($E<$ 2.5 eV) are obtained from the ground state by intraligand charge transfer (ILCT) located on the LH_2 ligand. More precisely, electronic density is shifted from the high-lying phenol orbitals toward the vacant π orbitals of the phenanthroline moiety. The corresponding transitions would range approximately from 490 to 600 nm with low intensity owing to the order of magnitude of their oscillator strengths. Here they are referred to as intraligand charge-transfer transitions (ILCTs) and are not assigned in the experimentally measured electronic absorption spectrum in solution. They most probably contribute to the feet of the more intense transitions occurring at higher energy. Furthermore, it is important to recall that the present calculations concern the isolated molecule and an exact correlation with the experimentally measured spectrum would be a far-fetched expectation.

The states obtained by charge transfer from the metal to the ligands lie at energies greater than 2.7 eV. Although some mixture occurs, metal-to-bipyridine charge transfers (abbreviated as MBCTs) and metal-to-phenanthroline charge transfers (MPCT excitations) result, to a first approximation, in distinct excited states. The population of the π_1^* orbitals of bipyridine is generally less energetic than that of ψ and χ of phenanthroline. One should also note that both intraligand transfers and ligand LH_2-to-bipyridine charge transfers (LBCT excitations) also occur in the same energy region. As is the case for state 18, their oscillator strength may be of the same magnitude as that for metal-to-ligand charge transfers, and they consequently contribute to the observed spectrum in the 400–480 nm region. This finding has also been mentioned by other authors in cases involving ruthenium complexes with mixed ligands.[18] Thus, assignment of a broad band to a single type of transition (here "MLCT") is a false oversimplification.

Higher-energy transitions are also reported in Table 3, but are not discussed here.

Excited triplet states: We must emphasise that these states are calculated in the optimised geometry of the ground state; that is to say, they correspond to vertical transitions from the ground state.

All T_n states with energy smaller than the excitation energies used in photophysical experiments (λ_{exc} = 532 nm, E_{exc} = 2.33 eV and λ_{exc} = 355 nm, E_{exc} = 3.49 eV) are susceptible to involvement in the deactivation processes. The first ten calculated triplet states are reported in Table 4. Triplet T_1 lies 0.14 eV lower than singlet S_1, so the first excited state of the complex is a triplet state. We notice that, starting from the ground electronic configuration, the first seven triplets are the results of intraligand or ligand–ligand charge transfers. The triplets with metal-to-ligand charge-transfer character are encountered at energies higher than 2.29 eV. This corresponds to the lower limit of 540 nm for an emissive deactivation process to the ground state in a vertical transition.

Table 3. Selected calculated singlet excited states S_n for $[(bpy)_2Ru(LH_2)]^{2+}$. Symmetry, excitation energy (E), corresponding wavelength (λ), oscillator strength (f), constituent monoexcitations from the ground state with their contribution in parentheses, dominant character.

Singlet state number n	Symmetry	E [eV]	λ [nm]	f	Constituent monoexcitations contributions[a]	nature	Dominant character of the excitation[b]
1	A	2.050	605	0.006	198→199 (0.96)	PhOH→π*(bpy)	LBCT
4	A	2.206	562	0.017	198→201 (0.94)	PhOH→ψ(phen)	ILCT
6	B	2.323	534	0.034	197→201 (0.49)	PhOH→ψ(phen)	ILCT
					198→202 (0.49)	PhOH→χ(phen)	
7	B	2.368	524	0.035	197→201 (0.51)	PhOH→ψ(phen)	ILCT
					198→202 (0.49)	PhOH→χ(phen)	
8	A	2.427	511	0.024	197→202 (1.00)	PhOH→χ(phen)	ILCT
11	A	2.520	492	0.014	196→199 (0.88)	salophen→π*(bpy)	LBCT
13	A	2.672	464	0.019	196→201 (0.71)	salophen→ψ(phen)	ILCT
					193→199 (0.16)	d_π(Ru)→π*(bpy)	
15	A	2.711	457	0.013	193→199 (0.50)	d_π(Ru)→π*(bpy)	MBCT
					196→201 (0.21)	salophen→ψ(phen)	
					196→199 (0.13)	salophen→π*(bpy)	
17	B	2.822	439	0.064	192→199 (0.58)	d_π(Ru)→π*(bpy)	MBCT
					193→200 (0.30)	d_π(Ru)→π*(bpy)	
18	B	2.860	434	0.138	196→202 (0.92)	salophen→ψ(phen)	ILCT
19	A	2.861	433	0.022	198→203 (1.00)	PhOH→π*(bpy)	LBCT
20	A	2.925	424	0.149	192→200 (0.69)	d_π(Ru)→π*(bpy)	MBCT
					193→201 (0.17)	d_π(Ru)→ψ(phen)	
					193→199 (0.14)	d_π(Ru)→π*(bpy)	
21	B	2.951	420	0.015	192→201 (0.96)	d_π(Ru)→ψ(phen)	MPCT
31	A	3.232	384	0.015	195→202 (0.45)	salophen→χ(phen)	ILCT
					192→202 (0.20)	d_π(Ru)→χ(phen)	
					193→201 (0.13)	d_π(Ru)→ψ(phen)	
					198→207 (0.12)	PhOH→imine	
32	A	3.239	383	0.052	198→207 (0.37)	PhOH→imine	ILCT
					194→202 (0.29)	d_π(Ru)→χ(phen)	
					192→202 (0.13)	d_π(Ru)→χ(phen)	
					193→201 (0.13)	d_π(Ru)→ψ(phen)	
33	B	3.292	377	0.025	193→202 (0.83)	d_π(Ru)→χ(phen)	MPCT
34	A	3.299	376	0.045	191→199 (0.65)	salophen→π*(bpy)	LBCT
					192→202 (0.14)	d_π(Ru)→χ(phen)	
35	B	3.299	376	0.012	197→206 (0.95)	PhOH→π*(bpy)	LBCT
37	A	3.319	374	0.097	192→202 (0.45)	d_π(Ru)→χ(phen)	MPCT
					191→199 (0.19)	salophen→π*(bpy)	
					195→202 (0.12)	salophen→χ(phen)	
					196→203 (0.10)	salophen→π*(bpy)	
38	B	3.325	373	0.030	198→208 (0.87)	PhOH→imine	ILCT
39	A	3.344	371	0.093	198→207 (0.30)	PhOH→imine	ILCT
					196→203 (0.25)	salophen→π*(bpy)	
					195→202 (0.19)	salophen→χ(phen)	
					194→202 (0.17)	d_π(Ru)→χ(phen)	
40	A	3.346	371	0.025	196→203 (0.65)	salophen→π*(bpy)	LBCT
					192→202 (0.11)	d_π(Ru)→χ(phen)	

[a] Only contributions larger than 0.10 are specified. [b] ILCT: intraligand charge transfer in the LH_2 ligand. LBCT: ligand–ligand charge transfer from ligand LH_2 to the bipyridines. MBCT: metal-to-ligand charge transfer from Ru to the bipyridines. MPCT: metal-to-ligand charge transfer from Ru to the phenanthroline part of the ligand LH_2.

As spin–orbit interactions are not considered in the TDDFT calculations, the results do not provide information on the triplet–singlet transition intensities. Such interactions will have two effects. Firstly, the "forbidden transitions" will gain in intensity and so emission will be observed. Secondly, the energy of the lowest triplet state will be lowered by coupling with higher singlets and triplets states. Nevertheless, the description in terms of singlet and triplet states remains reasonable in the case of ruthenium complexes, as is detailed later.

Lowest triplet state of $[(bpy)_2Ru(LH_2)]^{2+}$ and $[Ru(bpy)_3]^{2+}$: In our previous paper we described a photophysical study of $[(bpy)_2Ru(LH_2)]^{2+}$. In the absence of an electron acceptor, fast quenching of the triplet state ($\tau < 100$ ps) occurs after laser excitation at 532 nm. On comparison with the emission characteristics of $[Ru(bpy)_3]^{2+}$, the experimental data suggested that this quenching is due to the ligand. In such a process the lowest excited state, which is a triplet, is susceptible to play a significant role and we now focus more attention on this state.

Spin-unrestricted calculations with full geometry optimisation at the UB3LYP/LanL2DZ level were employed to in-

Table 4. First triplet excited states T_n for $[(bpy)_2Ru(LH_2)]^{2+}$ calculated at the ground-state geometry. Symmetry, excitation energy (E), corresponding wavelength (λ), constituent monoexcitations from the ground state with their contribution in parentheses, dominant character of the excitation.

Triplet-state number n	Symmetry	E [eV]	λ [nm]	Constituent monoexcitations contributions[a]	nature	Dominant character of the excitation[b]
1	B	1.912	649	198→202 (0.67)	PhOH→χ(phen)	ILCT
				196→202 (0.28)	salophen→χ(phen)	
2	A	2.016	615	198→199 (0.67)	PhOH→π^*(bpy)	LBCT
				198→201 (0.28)	PhOH→ψ(phen)	
3	A	2.119	585	198→201 (0.54)	PhOH→ψ(phen)	ILCT
				198→199 (0.35)	PhOH→π^*(bpy)	
4	B	2.139	580	198→200 (0.97)	PhOH→π^*(bpy)	LBCT
5	B	2.171	571	197→199 (0.93)	PhOH→π^*(bpy)	LBCT
6	A	2.218	559	197→202 (0.64)	PhOH→χ(phen)	ILCT
				197→200 (0.16)	PhOH→π^*(bpy)	
7	A	2.265	547	197→200 (0.71)	PhOH→π^*(bpy)	LBCT
				197→202 (0.12)	PhOH→χ(phen)	
				194→200 (0.12)	d_π(Ru)→π^*(bpy)	
8	A	2.290	542	194→200 (0.63)	d_π(Ru)→π^*(bpy)	MBCT
				195→200 (0.20)	salophen→π^*(bpy)	
				197→200 (0.17)	PhOH→π^*(bpy)	
9	B	2.316	535	197→201 (0.67)	PhOH→ψ(phen)	ILCT
				196→202 (0.18)	salophen→χ(phen)	
10	B	2.320	535	194→199 (0.66)	d_π(Ru)→π^*(bpy)	MBCT
				195→199 (0.21)	d_π(Ru)→π^*(bpy)	

[a] Only contributions larger than 0.10 are specified. [b] ILCT: intraligand charge transfer in the LH_2 ligand. LBCT: ligand–ligand charge transfer from ligand LH_2 to the bipyridines. MBCT: metal-to-ligand charge transfer from Ru to the bipyridines. MPCT: metal-to-ligand charge transfer from Ru to the phenanthroline part of the ligand LH_2.

vestigate this T_1 state for **Ru-L**, as well as for **Ru-bp** for comparison. We have described the calculated geometries above. The electronic structures discussed below are based on the energy level diagrams, nature of the triplets' spin-orbitals and spin density distributions. We first consider $[Ru(bpy)_3]^{2+}$ as a test for the methodology and also as a reference point.

$^3A_2$ state of $[Ru(bpy)_3]^{2+}$: Starting from the D_3 symmetry of the molecule in its ground state, a $^3A_2$ state is found as the lowest triplet state in this group. This high symmetry was initially retained because it prevents intensive orbital mixings and therefore allows clearer comparison between ground and excited states. Furthermore, computation time decreases substantially when symmetry is explicitly used in the programs. A consequent geometry optimisation of the $^3A_2$ state in C_2 symmetry was performed and led to a slightly stabilised ^3B state ($\approx$0.2 eV). Nevertheless, the groups of orbitals in the energy level diagram retained large similarities. It is not to be excluded, however, that an excited triplet in D_3 could experience such a large drop in energy in the C_1 symmetry as to fall as the lowest triplet. Here, too, an extensive description of the low-lying states of ruthenium tris-bipyridine is not essential for our study, so we focus on the $^3A_2$ state. Its calculated energy is 2.32 eV above the $^1A_1$ state in the ground-state geometry and 2.23 eV after relaxation in D_3 symmetry. This energy gives a maximum value of 557 nm for a radiative decay to the ground state, as compared to the experimental value of 610 nm. No substantial change, either for the energies or for the character of the orbitals, is computed in this limited geometry optimisation.

For $[Ru(bpy)_3]^{2+}$, Figure 4 presents the energy correlations between the $^3A_2$ spin-orbitals and the $^1A_1$ MOs. On going from S_0 to T_1, the α vacant π_1^*(bpy) spin-orbital of *a2* symmetry is stabilised and therefore accepts one electron, whilst the β occupied d_π(Ru) spin-orbital of *a1* symmetry rises in energy and is depopulated. Effectively, a $d_\pi(a1)\rightarrow\pi_1^*(a2)$ electron transfer is achieved to generate this lowest $^3A_2$ excited state. The nature of this transition and of this lowest triplet state is in agreement with the DFT results of Daul.[22]

As can be seen in Figure 5, the involved spin-orbitals $\pi_1^*(a2)\alpha$ and $d_\pi(a1)\beta$ retain the same character and electron distribution as in the $^1A_1$ state, so the lowest triplet state in $[Ru(bpy)_3]^{2+}$ is well known as a metal-to-ligand charge transfer state. The resulting spin density is represented in Figure 6, which shows that approximately one spin is located on the ruthenium while the other is equally distributed over the three coordinated bipyridines. The energy level diagram also indicates that all types of occupied orbitals, except for d_π, retain nearly the same energy as in the ground state. The metallic orbitals are strongly stabilised (mean value 1.6 eV), which indicates that ruthenium is now in a higher oxidation state—formally Ru^{III}—as a consequence of the electron transfer. In D_3 symmetry, the $^3A_2$ state is thus the "charge-separated state", which can be formulated as $[Ru^{III}(bpy^{[\bullet-]1/3]})_3]^{2+}$ in a totally delocalised description. This point is further discussed in a subsequent section.

Another consequence of the lowering of the d orbitals is that their energies become of the same order as those of the occupied π(bpy) orbitals, thus allowing a certain mixing, as is the case for the β spin-orbitals of *e* symmetry (Figure 5).

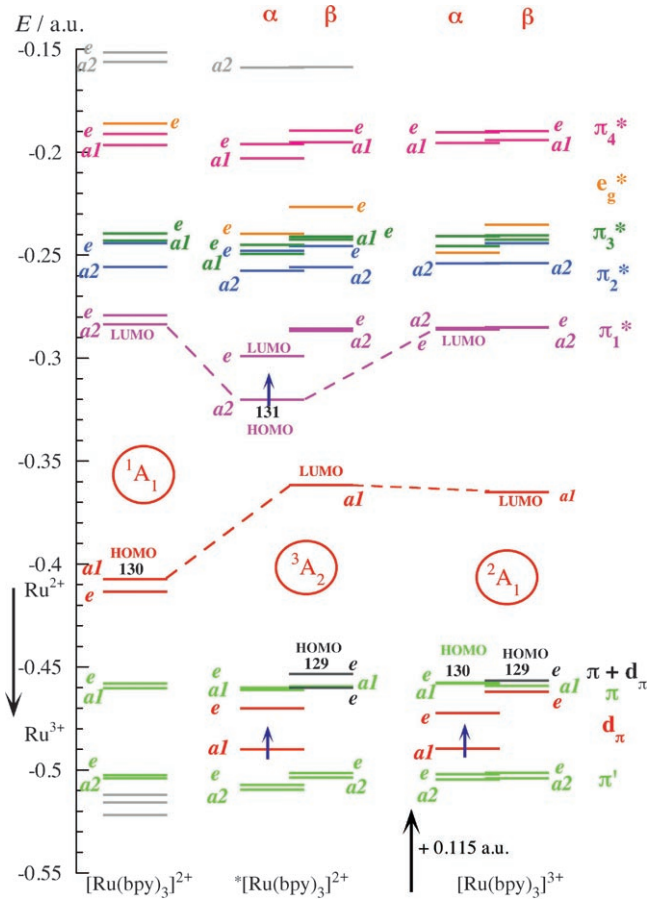

Figure 4. Energy level diagram (in atomic units: a.u.) of frontier orbitals for $[Ru(bpy)_3]^{2+}$ in the $^1A_1$ (left) and $^3A_2$ (middle) states and for $[Ru(bpy)_3]^{3+}$ $^2A_1$ (right). The energy levels for $[Ru(bpy)_3]^{3+}$ are shifted by 0.115 a.u. to allow for the +3 charge of this molecule in relation to the +2 for the two other states (see text). Orbitals resulting from important mixing are dark grey. The blue arrows indicate the approximately uncompensated α spins.

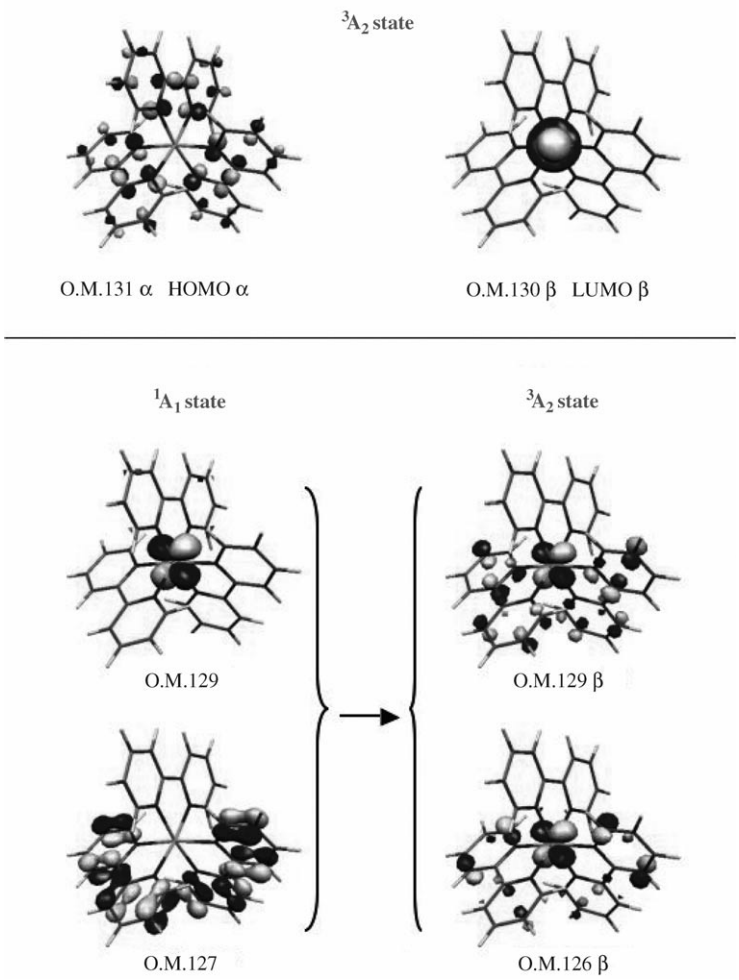

Figure 5. Selected orbitals of $[Ru(bpy)_3]^{2+}$. Top: HOMO α and LUMO β in the $^3A_2$ state of $[Ru(bpy)_3]^{2+}$. Bottom: Mixing of the *e*-symmetry d_π and π(bpy) MO of the $^1A_1$ state into corresponding *e*-symmetry β spin-orbitals in the $^3A_2$ state.

^3B state of $[(bpy)_2Ru(LH_2)]^{2+}$: We will now analyse the lowest triplet state of **Ru-L** by the same approach. However, because of the larger size and the lower symmetry of the system, the orbital energy levels are closer to each other and so are susceptible to mixing. We may therefore expect that the orbitals will no longer retain a relative pure character such as seen in the ground state.

The energy level diagram for the frontier spin-orbitals of the T_1 state—found to be a ^3B state—in connection with the MOs for the ^1A state are presented in Figure 7. They are derived through consideration of the optimised geometries for both states.

As we have discussed in the molecular structures section, the geometries are notably different in the two states. If some spin-orbitals are easily related to molecular orbitals in the singlet state, others (shown in grey) are the result of orbital mixing. This is clearly the case for the HOMO α of *a* symmetry and the LUMO β of *b* symmetry shown in Figure 8. The former is a combination of phenanthroline (MO 202 χ(phen)) and imine (MO 208) orbitals, whilst the

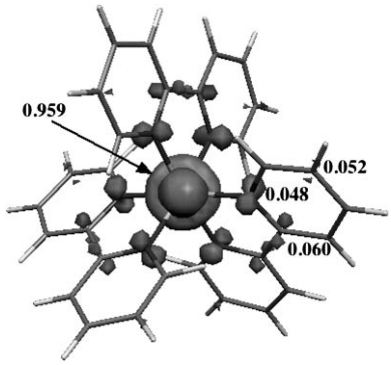

Figure 6. Spin density distribution for $[Ru(bpy)_3]^{2+}$ in the $^3A_2$ state.

latter originates from the salophen orbital 196, with a minor contribution from MO 198. It must be pointed out that no metallic contribution is present. The virtual electron transfer involved in generating the lowest triplet state from the ground state is therefore an intraligand charge transfer

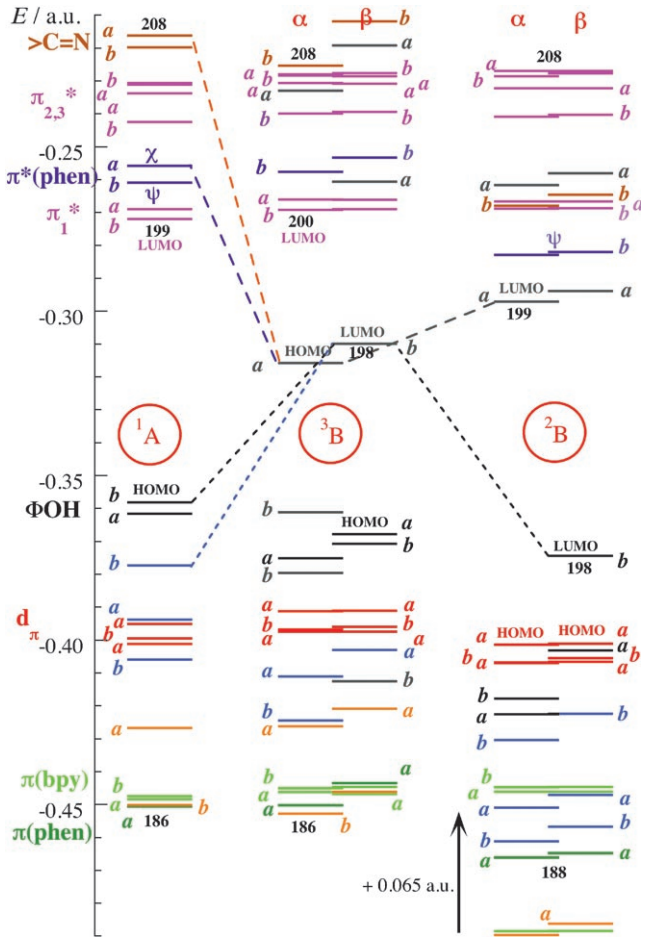

Figure 7. Energy level diagram (in atomic units: a.u.) of frontier orbitals for $[(bpy)_2Ru(LH_2)]^{2+}$ in the ^1A (left) and ^3B (middle) states and for $[(bpy)_2Ru(LH_2)]^{3+}$ ^2B (right). Orbitals resulting from important mixing are shown in dark grey. The energy levels for $[(bpy)_2Ru(LH_2)]^{3+}$ are shifted by 0.065 a.u. to allow for the +3 charge of this molecule in relation to the +2 for the two other states (see text).

(ILCT) in the bichromophoric phenanthroline-salophen ligand.

The ^3B state in its optimised geometry is calculated to be 1.56 eV above the ground sate in the ^1A geometry. The spin density distribution (Figure 9) is spread out over the whole LH_2 ligand. With regard to atomic spins (difference on each atom of the α and β electronic populations), it can be seen that about one unpaired α spin is located on the phenanthroline moiety and the other is borne by the two -N=C-C_6H_4-OH arms of the salophen moiety. This situation reflects the intraligand electronic transfer leading to this ^3B state and is totally different from a conventional charge-separated state picture in excited ruthenium complexes. The spin density of the lowest triplet state of the free ligand LH_2, also indicated in Figure 9, supports the notion that the lowest triplet state of **Ru-L** is in fact that of the ligand. It is hence not surprising that both the free ligand and the complex adopt the same distorted structure of the phenanthroline moiety in their lowest triplet state, as depicted in the structure section. Figure 8 shows that depopulation of LUMO β decreases the π bonding character in the C6–C6′ and N2–C7 bonds and suppresses the antibonding overlap in C6–N2. The first two bonds are thus lengthened and the last one shortened in the triplet state, as reported in Table 1.

Oxidised ruthenium complexes: To shed light on the photo-induced charge shift (PICS) processes of the ruthenium complexes, we have to consider different available ways of deactivation of the photoexcited triplet states. It is well established that in presence of an electron acceptor such as methyl viologen, oxidative quenching gives rise to the oxidised complex. $[Ru(bpy)_3]^{3+}$ and $[(bpy)_2Ru(LH_2]^{3+}$ were therefore studied. Calculations were performed on the ground doublet states and the geometries were optimised at the UB3LYP/LanL2DZ level in D_3 and C_2 symmetry, respectively. The most important feature concerning the structures is that the phenanthroline is no longer distorted in the oxidised **Ru-L** complex, as indicated by the value of the dihedral N2′-C6′-C6-N2 of 1.6°, as compared to 31.2° in the triplet state.

$[Ru(bpy)_3]^{3+}$: The ground state of the oxidised complex is a $^2A_1$ state. The energy levels diagram for $[Ru(bpy)_3]^{3+}$ (Figure 4) is stabilised overall by about 0.115 a.u. (≈3.13 eV) relative to that for $[Ru(bpy)_3]^{2+}$ in the $^3A_2$ state, due to the increase in molecular positive charge. This value was chosen in order to assign the same energy to the vacant

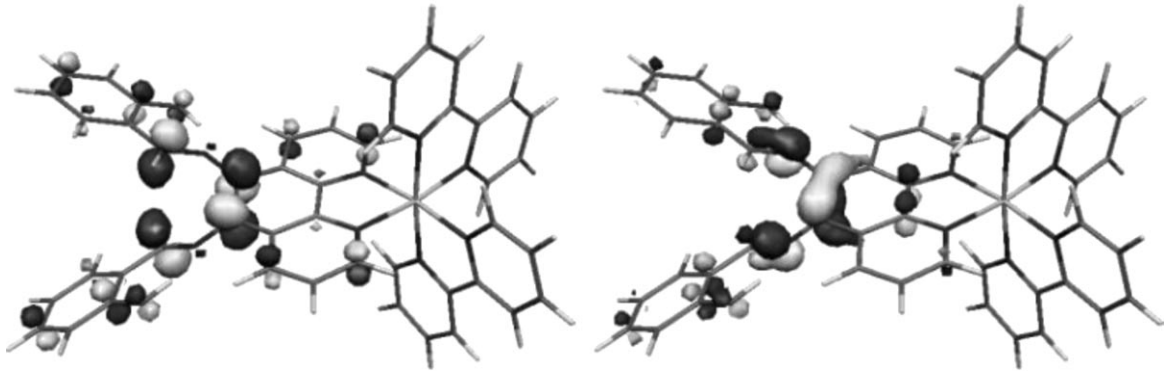

Figure 8. HOMO α (left) and LUMO β (right) of $[(bpy)_2Ru(LH_2)]^{2+}$ in the lowest ^3B state.

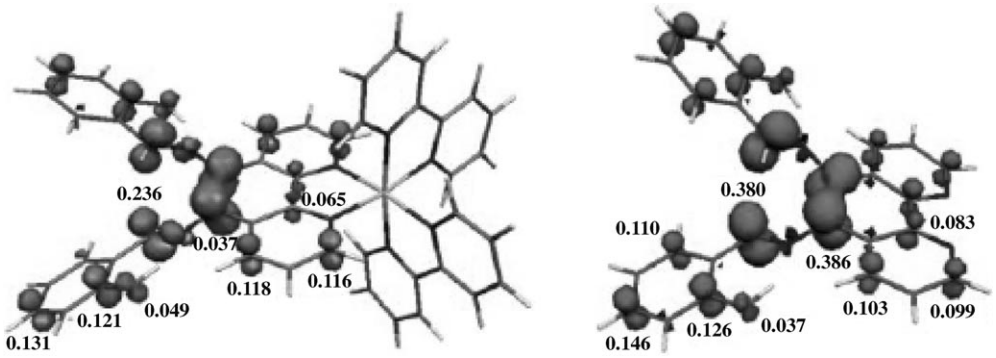

Figure 9. Spin density distribution for $[(bpy)_2Ru(LH_2)]^{2+}$ in the lowest ^3B state (left) and for LH_2 in the ^3B state (right).

π_1*(bpy) orbitals in $[Ru(bpy)_3]^{3+}$ and in $[Ru(bpy)_3]^{2+}$ (both in the $^1A_1$ and $^3A_2$ states), by the strategy explained above. Apart from this overall translation, the energy diagrams of spin-orbitals for $^2A_1$ and $^3A_2$ are very similar. The main difference concerns the α π_1*(bpy) spin-orbital of *a2* symmetry, which rises in energy and is now vacant (LUMO α). The compositions of the other orbitals are only slightly affected. Consequently, the spin density in this $^2A_1$ state is totally localised on the ruthenium, which is formally Ru^{III}, whilst the bipyridine ligands remain (also formally) uncharged.

These findings are also supported on consideration of the calculated Mulliken charges on each fragment. These are collected in Table 5 for the S_0 and T_1 states of the complexes (Figure 7) differs strongly from that of the ^3B state. Surprisingly, as a general rule the spin-orbitals of the ruthenium and the bpy ligands retain almost the same character and the same energy (after energy shift) while those of the LH_2 ligand are stabilised. This computational evidence indicates that the LH_2 ligand has gained a positive charge by removal of one electron. Formally, ruthenium remains Ru^{II}. The spin density distribution is mainly the α counterpart of the β (vacant) LUMO, as shown in Figure 10.

The computed Mulliken charges reported in Table 5 clearly illustrate that the formal oxidation state of the ruthenium remains the same in all states. Furthermore, on going from S_0 to T_1, the bpy moieties retain nearly the same charge, and (negative) electron density is transferred from the -N=C-C_6H_4-OH arms to the phenanthroline moiety. In the oxidised complex, from the total charge increase of one, only 0.06 is allocated to each bipyridine, 0.16 to the phenanthroline and 0.36 to each pending phenol group. This finding is in total agreement with the experimental results of differential pulsed cyclic voltammetry, which assign the first anodic wave to the oxidation of the phenol.

Table 5. Mulliken charges for different fragments of ligand LH_2, $[Ru(bpy)_3]^{2+}$ and $[(bpy)_2Ru(LH_2)]^{2+}$ in the singlet and triplet states, as well as for the oxidised form.

Molecule	Fragment	[ ]		$[ ]^{2+}$		$[ ]^{3+}$
		S = 0	S = 1	S = 0	S = 1	S = ½
Ru-bp	Ru			0.891	0.976	0.964
	bpy			0.370	0.341	0.679
Ru-L	Ru			0.898	0.894	0.903
	bpy			0.350	0.345	0.411
	phen			0.296	0.174	0.464
	-N=C-C_6H_4-OH			0.054	0.121	0.405
LH_2	phen	0.134	0.111			
	-N=C-C_6H_4-OH	−0.067	−0.056			

as well as for the oxidised forms. In the dicationic species, the Mulliken charges are approximately 0.89 for a formal Ru^{II} and 0.98 for a formal Ru^{III}, a small variation, due to changes in π back-bonding and covalency effects. Hence, on going from $^1A_1$ to the charge-separated state $^3A_2$, transfer of electronic density on each bipyridine decreases the positive charge of each ligand by only 0.03 (and not by 0.33 as suggested by the $[Ru^{III}(bpy^{[\bullet-]1/3})_3]^{2+}$ formulation). In the oxidised $^2A_1$ state, the Mulliken charge of Ru^{III} remains almost the same (0.96), but each ligand experiences a charge increase of nearly one third of that of the molecule.

$[(bpy)_2Ru(LH_2)]^{3+}$: For **Ru-L**, the overall stabilisation determined by the same criterion as above is about 0.065 a.u. ($\approx$1.67 eV). The energy diagram of the oxidised ^2B state

Interpretation of photophysical properties of $[Ru(bpy)_3]^{2+}$ and $[(bpy)_2Ru(LH_2)]^{2+}$

$[Ru(bpy)_3]^{2+}$ has been extensively studied as a model for Ru-polypyridine complexes. The large number of works devoted to the study of the ground state and the lowest excited states of this system has allowed an understanding of the photophysical properties to be gained. Laser excitation results in ^{1}MLCT metal-to-ligand excited singlet state(s). Ultrafast singlet→triplet excited state conversion (intersystem crossing) occurs with a time constant of a few tenths of a fs,[31] but about a hundred femtoseconds seems to be the overall timescale for formation of the ^{3}MLCT set.[32,33] The

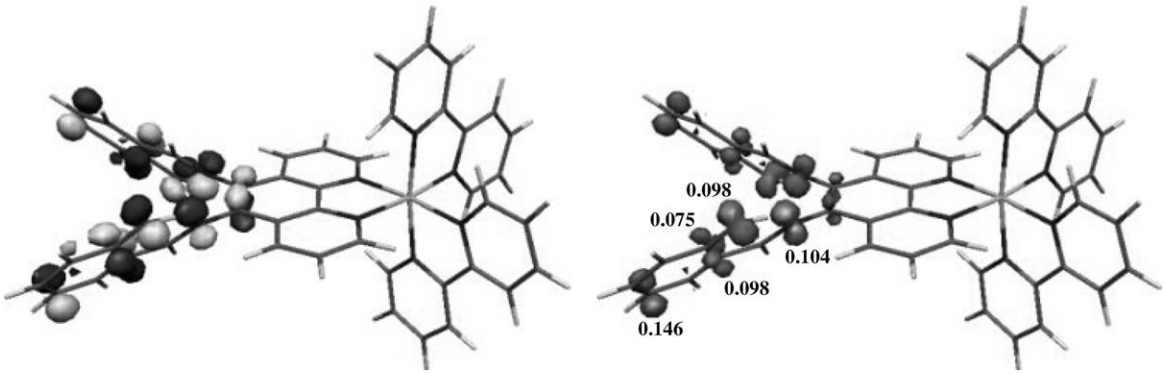

Figure 10. LUMO β (left) and spin density distribution (right) for $[(bpy)_2Ru(LH_2)]^{3+}$ in the ^2B state.

quantum yield of formation of these states is close to unity,[34] so relaxation processes are dominated by decay of the triplets rather than by spin-allowed fluorescence or internal conversion from ^{1}MLCT. From time-resolved luminescence measurements at 610 nm, the emission lifetime at room temperature—about 800 ns depending on sample conditions—has been obtained. Temperature dependence studies of the mean lifetime have also been performed to ascertain the energy level splittings of the decaying states in thermal equilibrium.[35]

Another experimental technique providing information on the excited state is the study of flash-induced absorption change spectra. It gives some precious insight into the electronic spectra of the state generated from the singlet state by laser excitation followed by ultrafast intersystem crossing. Experimental data concerning $[Ru(bpy)_3]^{2+}$, essentially in the middle-visible and IR regions, have been reported in the past.[36,37] More recently, Shimizu et al.[38] have obtained the near-IR absorption, which shows a broad band (700 to 1300 nm) peaking at 900 nm. We have also commented on such data in the 400–1000 nm range for **Ru-bp** and **Ru-L** in our previous paper. We will now attempt to compare these experimental results with theoretical ones in the case of ruthenium tris-bipyridine.

Absorption spectrum of the triplet state of $[Ru(bpy)_3]^{2+}$: From the optimised $^3A_2$ state of $[Ru(bpy)_3]^{2+}$, TDDFT formalism allowed us to calculate the absorption transitions for the triplet in the near-infrared and the visible region.

Our results are presented in Table 6. As the charge-separated states involve a Ru^{III} ion along with bipyridine(s) in a partially or totally reduced form, assignments of absorptions of these excited species have generally been achieved by comparison with the spectra of the oxidised and reduced complexes (or reduced ligand) as discussed, for instance, by McCusker.[39] We also report our calculated absorption spectra of the oxidised complex $[Ru(bpy)_3]^{3+}$ and the $(bpy)^-$ ion, obtained by the same procedure, in Table 6.

Two types of transitions can be considered, depending on whether α or β spin-orbitals are involved. The first class concerns excitations from $\pi_1^*(a_2)$ to higher vacant orbitals of the bipyridine ligands and so are ligand-centred (LC). They are reminiscent of the transitions for the $(bpy)^-$ ion. As can be read from Table 6, each $\pi_1^*\rightarrow\pi_i^*$ transition for the free bipyridine anion gives rise within **Ru-bp** in D_3 symmetry to two excitations—$\pi_1^*\rightarrow\pi_i^*(a1)$ and $\pi_1^*\rightarrow\pi_i^*(e)$—which are fairly well separated (the $\pi_1^*\rightarrow\pi_2^*$ transition at 1154 nm in $(bpy)^-$, for instance, yields the *a1* and *e* transitions at 1251 and 999 nm, respectively, in the $^3A_2$ state of the complex). These findings are thus more likely to support the origin of the broad absorptions in the NIR region. Indeed, the $\pi_1^*\rightarrow\pi_{2,3}^*$ transition ($\pi_7\rightarrow\pi_{8,9}$ in a more conventional notation) was predicted to occur around 910 nm by Braterman and was assigned around 900 nm for a coordinated $(bpy)^-$ in the localised $[Ru^{III}(bpy)_2(bpy)^-]^{2+}$ structure by Shimizu. Our $[Ru^{III}(bpy^{[\bullet-]1/3})_3]^{2+}$ delocalised description yields these transitions in the same region, but with a larger span.

The second type of transitions concerns excitations to $d_\pi(a_1)$. They originate from π or π′ orbitals of the bipyridine and are thus essentially assigned as ligand-to-metal charge transfers (LMCTs). However, it is important to note that, owing to the reduction in the energy of the d_π orbitals of Ru^{III}, they mix strongly with the π orbitals, as shown in Figure 5. Consequently, these transitions acquire a substantial metal-centred (MC) character (d_π to d_π and not dd, as is often understood from this abbreviation). Moreover, Table 6 shows that these transitions are strikingly similar to those of $[Ru(bpy)_3]^{3+}$. The presence of Ru^{III} in the $^3A_2$ state is outstandingly apparent. Our theoretical data therefore allow us to highlight the nature of the LMCT transitions. Furthermore, no charge transfer from metal to ligand was calculated above 400 nm, in contrast with Braterman's proposition of a transition near 450 nm. This is readily explained by the fact that the occupied d_π orbitals of Ru^{III} are highly stabilised and MLCT transitions are hence more energetic.

The calculated spectrum (only above 350 nm) of the optimised $^1A_1$ state is reported in Table 7. From the results in Table 6 and Table 7, theoretical stick spectra have been reproduced from the excitation energies and oscillator strengths. The simulated spectra were then obtained by convolution of each transition with a Gaussian function of bandwidth at half-height of 3200 cm^{-1} along with area under the curve proportional to f and by summation of all these features. The value of 3200 cm^{-1} was chosen because it usu-

Table 6. Selected calculated absorptions of the $^3A_2$ state of $[Ru(bpy)_3]^{2+}$, the $^2A_1$ state of $[Ru(bpy)_3]^{3+}$ and the doublet state of the $(bpy)^-$ anion in the NIR/Vis region.

	Excited state number	E [eV]	λ [nm]	Symmetry of the transition[a]	f	Dominant monoexcitation[b]	Character[c]
$[Ru(bpy)_3]^{2+}$	5	0.991	1251	A_1	0	$\pi_1^*(a_2)\alpha\rightarrow\pi_2^*(a_1)\alpha$	LC
	6	1.238	1001	A_2	0.011	$\pi_1^*(a_2)\alpha\rightarrow\pi_3^*(a_1)\alpha$	LC
	7, 8	1.241	999	E	0.001	$\pi_1^*(a_2)\alpha\rightarrow\pi_2^*(e)\alpha$	LC
	9, 10	1.312	945	E	0.002	$\pi_1^*(a_2)\alpha\rightarrow d_\sigma^*(e)\alpha$	LMCT
	11, 12	1.372	904	E	0.009	$\pi_1^*(a_2)\alpha\rightarrow\pi_3^*(e)\alpha$	LC
	13, 14	1.819	682	E	0.007	$d_\pi+\pi(e)\beta\rightarrow d_\pi(a_1)\beta$	MC+LMCT
	15	1.875	661	A_1	0	$\pi(a_1)\beta\rightarrow d_\pi(a_1)\beta$	LMCT
	16	2.569	483	A_2	0.064	$\pi_1^*(a_2)\alpha\rightarrow\pi_4^*(a_1)\alpha$	LC
	17, 18	2.734	454	E	0.017	$\pi_1^*(a_2)\alpha\rightarrow\pi_4^*(e)\alpha$	LC
	19	2.968	418	A_2	0.009	$\pi'(a_2)\beta\rightarrow d_\pi(a_1)\beta$	LMCT
	20, 21	3.001	413	E	0.014	$\pi'(e)\beta\rightarrow d_\pi(a_1)\beta$	LMCT
$[Ru(bpy)_3]^{3+}$	3, 4	1.746	710	E	0.003	$d_\pi+\pi(e)\beta\rightarrow d_\pi(a_1)\beta$	MC+LMCT
	5	1.781	696	A_1	0	$\pi(a_1)\beta\rightarrow d_\pi(a_1)\beta$	LMCT
	6, 7	2.908	426	E	0.016	$\pi'(e)\beta\rightarrow d_\pi(a_1)\beta$	LMCT
	8	2.910	426	A_2	0.006	$\pi'(a_2)\beta\rightarrow d_\pi(a_1)\beta$	LMCT
$(bpy)^-$	1	1.074	1154	A_1[d]	0.000	$\pi_1^*\alpha\rightarrow\pi_2^*\alpha$	LC
	2	1.490	832	B_2	0.007	$\pi_1^*\alpha\rightarrow\pi_3^*\alpha$	LC
	3	2.968	489	B_2	0.158	$\pi_1^*\alpha\rightarrow\pi_4^*\alpha$	LC

[a] A_2 transitions are z-polarised and E transitions are x,y-polarised; A_1 transitions are forbidden. [b] $\pi_i^*(\gamma)$: γ-symmetry MO of $[Ru(bpy)_3]^{2+/3+}$, which is approximately constructed from the π_i^* vacant orbitals of the 3 bpy (neglecting ligand–ligand interaction). [c] LC: ligand-centred transition. MC: metal-centred transition. LMCT: ligand-to-metal charge transfer. [d] In point group C_{2v}.

Table 7. Selected calculated absorptions of the $^1A_1$ state of $[Ru(bpy)_3]^{2+}$ in the NIR/Vis region.

Excited singlet-state number	E [eV]	λ [nm]	Symmetry of the transition	f	Dominant monoexcitation	Character[a]
1	2.522	492	A_2	0.002	$d_\pi(a_1)\rightarrow\pi_1^*(a_2)$	MLCT
5, 6	2.738	453	E	0.009	$d_\pi(e)\rightarrow\pi_1^*(a_2)$	MLCT
7, 8	2.887	430	E	0.109	$d_\pi(e)\rightarrow\pi_1^*(e)$	MLCT
10	3.372	368	A_2	0.008	$d_\pi(a_1)\rightarrow\pi_2^*(a_2)$	MLCT

[a] MLCT: metal-to-ligand charge transfer.

ally gives molar extinction coefficients consistent with experimentally measured ones for such large complexes. The "simulated" triplet state is shown in Figure 11.

The difference absorption spectrum for an isolated molecule was then calculated by subtraction between the spectra of the triplet and singlet states (Figure 11). The spectral morphology agrees nicely with experiment, although some shifts are observed. Even in view of the approximations of the theoretical method and the huge size of the computations, it is stimulating to acknowledge the excellent agreement between experimental and theoretical data. However, this remarkable computed finding must be regarded with caution, as contributions of other ^{3}MLCT states have not been considered. Nevertheless, it seems more likely that these states should have closely similar spectra. In this regard our results strongly support the totally delocalised description of the triplet state to reproduce the flash-induced absorption change spectrum of **Ru-bp**. We have demonstrated that, to reproduce the absorption features in the 700–1000 nm region, it is not necessary to imply a totally reduced $(bpy)^-$ ion along with a localised $[Ru^{III}(bpy)_2(bpy)^-]^{2+}$ formulation, as invoked in the past.[36,37,40] Nonetheless, we cannot exclude the description of a localised state with such a spectrum. Indeed, it is probable that both states would absorb around the same energies.[41] We comment later on delocalised/localised descriptions.

Photophysical properties of $[(bpy)_2Ru(LH_2)]^{2+}$: In the first place, it is perhaps necessary to summarise the experimental results. The luminescence of **Ru-L** at 610 nm was characterised by a biexponential decay. The dominant fast phase ($\tau <$ 100 ps), not well resolved at our experimental timescale, is absent for **Ru-bp** under the same experimental conditions and the slow component is characterised by a lifetime of about 800 ns as in **Ru-bp**. Comparison of the emission characteristics of the two complexes suggests that the observed quenching is related to the presence of the extended ligand LH_2.

Spectra of flash-induced absorption changes on excitation at 450 nm have been recorded for **Ru-bp** and **Ru-L**. Both complexes exhibit bleaching of the ground state absorption centred around 450 nm and broad absorption bands in the near-IR region. Nevertheless, if absorption increases are of the same order in the 700–1000 nm region, the bleaching at 450 nm for $[(bpy)_2Ru(LH_2)]^{2+}$ is only one fifth of that for $[Ru(bpy)_3]^{2+}$. Furthermore, the absorption changes for **Ru-bp** disappear with the same kinetics as the luminescence (800 ns), while the decay for **Ru-L** is much slower (about 30 μs). These contrasting observations suggest that the absorption changes for the latter complex are not related to

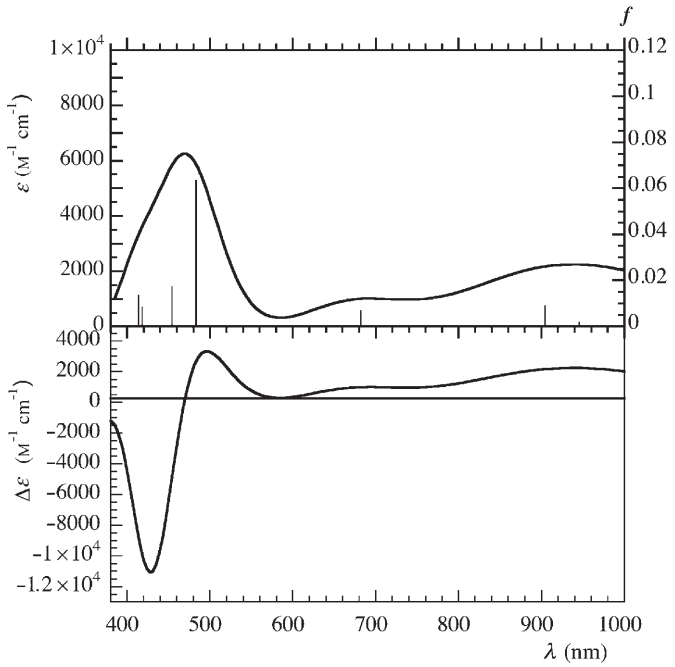

Figure 11. Theoretical spectra for $[Ru(bpy)_3]^{2+}$ in the Vis/NIR region. Top: Triplet state stick-spectrum calculated from the excitation energies and oscillator strengths f and simulated spectrum obtained by convolution with Gaussian line shapes of total bandwidth at half-height 3200 cm^{-1}. Bottom: Absorption change spectrum.

the MLCT state as is the case with ruthenium tris-bipyridine.

In the light of our theoretical calculations, we now propose some explanations of the photophysical results for $[(bpy)_2Ru(LH_2)]^{2+}$. Experimentally, the singlet states are reached upon laser excitation at $\lambda = 450$ nm. From Table 3 it can be seen that absorptions in this spectral window concern metal-to-ligand charge transfers (both on bpy and LH_2) and also an intense intraligand transfer in the core of LH_2. The ^{1}MLCT states are generated by exactly the same displacement of electronic density as in $[Ru(bpy)_3]^{2+}$ and will also give rise to ^{3}MLCT states by intersystem crossing. Starting from this set of triplet levels, the deactivation process can follow two pathways. Firstly, in these ^{3}MLCT states, the ruthenium is formally Ru^{III} with a local unpaired spin. Hence, spin–orbit coupling is able to couple these triplets with the singlet ground state, and radiative luminescent decay may occur with roughly the same kinetics as in **Ru-bp** (slow component). In **Ru-L**, however, another route for deactivation exists, due to the presence of triplet states lower in energy than the ^{3}MLCT states. As transitions from the ^{3}MLCT states to other triplet states are spin-allowed, ultrafast decay can occur and quench the emission (fast component), resulting in the lowest triplet state ^{3}B. As we have shown that no spin density is present on the heavy atom in this ^{3}ILCT state, spin–orbit interactions are hence inefficient to produce mixing with the singlet ground state. Consequently, the depopulation of ^{3}B will follow a nonradiative process. This finding accounts for the remarkable long lifetime of this excited state (30 μs).

As shown, a path of decay different from the luminescence of the ^{3}MLCT set is present in $[(bpy)_2Ru(LH_2)]^{2+}$, so the photophysics of this compound are consequently more intricate than those of ruthenium tris-bipyridine. Triplet states characterised by very different photophysical properties but also associated with extended ligands have been found in, for instance, $[(bpy)_2Ru(dppz)]^{2+}$ (dppz = dipyridophenazine).[42] The role of a low-lying ligand-centred triplet state has also been theoretically established by Pourtois et al.[11] in $[(phen)_2RuL]^{2+}$ complexes in which L is an extended polyaromatic ligand such as dipyridophenazine or tetrapyridophenazine. The lowest triplet is similarly found to be that of the free ligand and lies about 0.2 eV lower than the lowest ^{3}MLCT state. Its involvement in the photophysical observations has been discussed. The main difference with **Ru-L** is that our ^{3}B state lies ca 0.4 eV under the lowest ^{3}MLCT and that both states are separated by several other non metal-centred triplets. Furthermore, the geometry of the ligand on the metal ion is totally modified in this lowest triplet state, which seems not to be the case in the complexes mentioned above.

Discussion

Conceptual description of ruthenium-polypyridine complexes in their fundamental and excited states has always been the matter of debate. Indeed, a considerable number of papers have been devoted to this area. Some reviews—although not recent—are well documented.[41,43,44] In this discussion we will confront our theoretical calculations with previous studies in order to clarify and comfort our approach. Three different points will be considered.

Spin–orbit interactions: It is well known that ruthenium possesses a rather large spin–orbit coupling constant ($\zeta_{4d} \approx 1000$ cm^{-1}[45]) and spin–orbit interactions are invoked to explain the singlet–triplet conversions which occur in photophysical processes. Despite this, all our calculations have been performed without consideration of these effects. Some justifications for the framework of our approach can be cited. Crosby and co-workers have derived a model often termed the "electron-ion parent coupling model",[46] in which spin–orbit interactions are considered. They used it to fit the temperature dependence of the lifetime of $[Ru(bpy)_3]^{2+}$.[35] Their conclusion was that the emission arises from three states close in energy in thermal equilibrium: an A_1 lowest state, an E state nearly degenerated and an A_2 state about 0.01 eV higher. Spin labelling of these states was found to be wholly inappropriate.[47] This conclusion has been criticised by Kober and Meyer.[45,48] In their "electronic structural model", which also includes spin–orbit coupling, the main outcome was that transitions in $[Ru(bpy)_3]^{2+}$ may be classified as being mainly to singlet or to triplet states, though appreciable mixing occurs. More recently, in a density functional study of the MLCT states of $[Ru(bpy)_3]^{2+}$, Daul and co-workers[22] have calculated that the lowest ex-

cited state is $^3A_2$ ($d_\pi(a1)\rightarrow\pi_1^*(a2)$ excitation), which splits through second-order spin–orbit interaction into A_1 (lower) and E components separated by only 19 cm^{-1} ($\approx$0.002 eV) and presenting at least 85% triplet character. Above $^3A_2$, state $^1A_2$ (which also results from $d_\pi(a1)\rightarrow\pi_1^*(a2)$ excitation) lies 336 cm^{-1} ($\approx$0.042 eV) above A_1 and possesses 77% singlet character. All other states are found at least 1500 cm^{-1} higher than A_1. Hence, neglect of spin–orbit interaction remains a valid approach to calculate the energies and main character of the excited states of ruthenium complexes, as done elsewhere.[11,19]

Delocalisation/localisation: One of the most intriguing properties of $[Ru(bpy)_3]^{2+}$, which has constantly fuelled scientific debate, is the intimate description of the charge-separated states. Two points of view on this subject are commonly proposed: the delocalised one and the localised one. Whether these states are best described in terms of a Ru^{III} ion together with an electron delocalised on three bipyridines or together with an electron localised on one bpy has been the subject of controversy. Until now, no clear-cut conclusion has emerged. On one hand, delocalisation is invoked. In a study of mixed ligand chelates, for instance, Crosby and coworkers[49] inferred that the excited charge-transfer states are best described as the molecular states in which the optical electron resides equally on the three ligands. In their interpretation of high-resolution emission spectra of ruthenium tris-bipyridine-derived complexes with bpy-h8 and bpy-d8, Braun et al.[50] have concluded that the lowest MLCT excited state is delocalised over the metal and the different ligands. On the other hand, different techniques have concluded that the charge-separated states are localised. This is the case for resonance Raman experiments,[51,52] at least at the nanosecond timescale.

In our opinion, localised and delocalised descriptions do not necessarily exclude each other, depending on the timescale of the technique used. Indeed, if starting from the vibrational trapped $[Ru^{III}(bpy)_2(bpy)^-]^{2+}$ situation, subsequent electron hopping from one bpy to another would dynamically restore a delocalised situation. Interligand electron transfer dynamics has been studied by picosecond Raman spectra on mixed-ligand complexes.[53] It was found that the major proportion of the electrons was localised on the lower energy ligand on a 30 ps or faster timescale. In the symmetric case of $[Ru(bpy)_3]^{2+}$, hopping of the electron, resulting in a dynamically delocalised situation, as in mixed-valence compounds, has been considered by several authors.[41,52] Electronic absorption experiments have attempted to detect an excited state intervalence transition, though without success until now. It must, however, be considered that, after the excitation, a lowering of the symmetry of the system may be generated under the influence of a perturbation such as—for instance—vibrations or solvent effects producing a localised situation. Finally, recent data derived from femtosecond absorption anisotropy studies on $[Ru(bpy)_3]^{2+}$[32] have been interestingly interpreted as evidence of a delocalised-to-localised transition: the initially excited state of D_3 symmetry evolves in about 60 fs to a state of C_2 symmetry. In this regard, the polarity of the solvent was shown to play an important role in such processes.[33]

Because the three bipyridine ligands are equivalent in the ground state, computed molecular orbitals in the D_3 symmetry of the complex are delocalised. In the subsequent calculations of higher energy states described in terms of excitations from occupied to virtual MOs, all bpy moieties will play exactly the same role. In our approach, no perturbation involving one of the ligands is present to alter the transition moments, so the totally symmetric $[Ru^{III}(bpy^{[\bullet-]1/3})_3]^{2+}$ description is obtained (see, for instance, reference [45]). Such a calculated picture may, however, be viewed as the statistical mean of three equivalent and equiprobable situations in which the electron is localised on one of the ligands. The same arguments also hold for **Ru-L** in the computed C_2 symmetry. Hence, within this symmetry, both bipyridines (and both phenolic arms) bear the same spin density in each of the triplet states. The ^{3}MBCT states are therefore delocalised on both bpy moieties and similarly, in the lowest ^{3}B state, equal spin density is spread over both N=C-C_6H_4-OH fragments. However, vibrations or solvent interactions will probably lower the C_2 symmetry and trap the unpaired spin distribution. This is even clearer if we consider the photoinduced charge shift experiment after laser excitation on **Ru-L** in the presence of an external electron acceptor: oxidation occurs on only one of the two phenol rings and the symmetric situation described in the oxidised compounds section is no longer pertinent.

Surroundings effects: One crucial point concerning our theoretical work is that the calculations have been performed on an isolated molecule in the gas phase. However, numerous experimental studies indicate that the photophysical properties of $[Ru(bpy)_3]^{2+}$ and related complexes strongly depend on the nature of the solvent. The surroundings of the molecule will perturb the energy level diagram for both the ground and the excited states. This is especially true because charge-transfer states are considered. Indeed, in a charge-separated state, electronic density is redistributed on the periphery of the chromophore. Polar solvent molecules will hence strongly solvate the complex and modify the electronic repartition. The nature of the molecular orbitals and their energies will be affected and consequently the states' energy diagram, along with absorption and emission properties. The effects of the surroundings could be especially strong for the oxidised $[(bpy)_2Ru(LH_2)]^{3+}$ molecule. Indeed, we have produced evidence that oxidation is localised on the phenol and, as is well established, deprotonation frequently follows, depending on pH and solvent. None of these repercussions is taken into account in the framework of a monomolecular approach.

Conclusion

We have used DFT calculations to describe the ground state of a $[(bpy)_2Ru(LH_2)]^{2+}$ complex derived from $[Ru(bpy)_3]^{2+}$ in which LH_2 is a ligand that can be viewed as a fused phenanthroline and a tetradentate Schiff base cavity. It emerges that, in each molecular orbital, the electronic density is located with little mixture on only one fragment of the molecule: the ruthenium ion, the two bipyridines, or the phen-like part or the imine-phenol moiety of the ditopic ligand. Subsequent TDDFT calculations have provided the energies and main characters of the first singlet and triplet states relevant to the interpretation of the absorption and emission properties of the system. The outstanding result is that both the lowest singlets and lowest triplets mainly originate from intraligand charge transfers (ILCTs) in the LH_2 ligand.

The lowest triplet state has been studied in depth by DFT, which has established that the phenanthroline adopts a distorted nonplanar geometry as in the triplet state of the free ligand and is about 0.7 eV more stable than the lowest more usually encountered metal-to-ligand charge transfer triplet state. This ^3B state results from an electron transfer from the -N=C-C_6H_4-OH fragments to the phenanthroline part in LH_2. It is hence not a charge-separated state, because the spin density is totally distributed on the ligand, with no contribution on the ruthenium ion, which remains Ru^{II}. Such an excited state arises because the two parts of the heteroditopic ligand are different in nature, with the usual π^*-accepting orbitals of phenanthroline and high-lying occupied orbitals of the phenol groups.

We have pointed out the major role of this low-lying triplet not involving the ruthenium centre. Deactivation of the ^{3}MLCT states toward this ^{3}ILCT state is responsible for the two remarkable photophysical properties of this complex: the quenching of the emission and the occurrence of a long-lived (30 μs) excited state. Although bimolecular systems have not been considered in our theoretical study, we have substantiated the experimental finding that, in the presence of an external electron acceptor, photoinduced charge shifts result in a $[(bpy)_2Ru(LH_2)]^{3+}$ complex oxidised on the phenol. Our DFT results have produced evidence that in the tricationic species the ruthenium ion remains formally Ru^{II} and the spin density is localised on the -N=C-C_6H_4-OH fragments.

Acknowledgements

This work was supported by the CNRS (Programme Energie, PRI4) and the CEA for the LRC project (LRC-CEA n°33 V). We thank the Centre Informatique National de l'Enseignement Supérieur at Montpellier (France) and the Institut du Développement et des Ressources en Informatique Scientifique at Orsay (France) for providing facilities for calculation.

[1] Y. Pellegrin, A. Quaranta, P. Dorlet, M.-F. Charlot, W. Leibl, A. Aukauloo, *Chem. Eur. J.* **2005**, *11*, 3698–3710.
[2] V. Balzani, A. Credi, M. Venturi, *Coord. Chem. Rev.* **1998**, *171*, 2–16.
[3] H. D. Gafney, A. W. Adamson, *J. Am. Chem. Soc.* **1972**, *94*, 8238–8239.
[4] A. J. Vlcek, *Electron Transfer in Chemistry*, Wiley-VCH, **2001**, p. 804–877.
[5] L. Sun, L. Hammarström, B. Åkermark, *Chem. Soc. Rev.* **2001**, *30*, 36–49.
[6] D. Burdinski, K. Wieghardt, S. Steenken, *J. Am. Chem. Soc.* **1999**, *121*, 10781–10787.
[7] B. Gholamkhass, H. Mametsuka, K. Koike, T. Tanabe, M. Furue, O. Ishitani, *Inorg. Chem.* **2005**, *44*, 2326–2336.
[8] F. Lachaud, A. Quaranta, Y. Pellegrin, P. Dorlet, M.-F. Charlot, S. Un, W. Leibl, A. Aukauloo, *Angew. Chem.* **2005**, *117*, 1560–1564; *Angew. Chem. Int. Ed.* **2005**, *44*, 1536–1540.
[9] D. S. Seneviratne, M. J. Uddin, V. Swayambunathan, H. B. Schlegel, J. F. Endicott, *Inorg. Chem.* **2002**, *41*, 1502–1517.
[10] S. I. Gorelsky, A. B. P. Lever, *Can. J. Anal. Sci. Spect.* **2003**, *48*, 93–105.
[11] G. Pourtois, D. Beljonne, C. Moucheron, S. Schumm, A. Kirsch-De Mesmaeker, R. Lazzaroni, J. L. Bredas, *J. Am. Chem. Soc.* **2004**, *126*, 683–692.
[12] A. D. Becke, *J. Chem. Phys.* **1993**, *98*, 5648.
[13] G. Albano, P. Belser, C. A. Daul, *Inorg. Chem.* **2001**, *40*, 1408–1413.
[14] S. R. Stoyanov, J. M. Villegas, D. P. Rillema, *Inorg. Chem.* **2002**, *41*, 2941–2945.
[15] K. Zheng, J. Wang, W. Peng, X. Liu, F. Yun, *J. Phys. Chem. A* **2001**, *105*, 10899–10905.
[16] K. Zheng, J. Wang, Y. Shen, W. Peng, F. Yun, *J. Comput. Chem.* **2002**, *23*, 436–443.
[17] M. E. Casida, C. Jamorski, K. C. Casida, D. R. Salahub, *J. Chem. Phys.* **1998**, *108*, 4439.
[18] J. E. Monat, J. H. Rodriguez, J. K. McCusker, *J. Phys. Chem. A* **2002**, *106*, 7399–7406.
[19] J. F. Guillemoles, V. Barone, L. Joubert, C. Adamo, *J. Phys. Chem. A* **2002**, *106*, 11354–11360.
[20] S. R. Stoyanov, J. M. Villegas, D. P. Rillema, *Inorg. Chem. Com.* **2004**, *7*, 838–841.
[21] S. I. Gorelsky, S. C. da Silva, A. B. P. Lever, D. W. Franco, *Inorg. Chim. Acta* **2000**, *300*, 698–708.
[22] C. Daul, E. J. Baerends, P. Vernooijs, *Inorg. Chem.* **1994**, *33*, 3538–3543.
[23] L. Yang, A. M. Ren, J. K. Feng, X. D. Liu, Y. G. Ma, H. X. Zhang, *Inorg. Chem.* **2004**, *43*, 5961–5972.
[24] P. J. Hay, *J. Phys. Chem. A* **2002**, *106*, 1634–1641.
[25] A. D. Becke, *Phys. Rev. A* **1988**, *38*, 3098.
[26] C. Lee, W. Yang, R. G. Parr, *Phys. Rev. B: Condensed Matter.* **1988**, *37*, 785.
[27] T. H. Dunning, Jr, P. J. Hay in *Modern Theoretical Chemistry, Vol. 3* (Ed. H. F. Schaefer, III), **1976**, pp. 1–28.
[28] P. J. Hay, W. R. Wadt, *J. Chem. Phys.* **1985**, *82*, 270–283.
[29] M. J. Frisch, G. W. Trucks, H. B. Schlegel, G. E. Scuseria, M. A. Robb, J. R. Cheeseman, V. G. Zakrzewski, J. A. Montgomery, Jr., R. E. Stratmann, J. C. Burant, S. Dapprich, J. M. Millam, A. D. Daniels, K. N. Kudin, M. C. Strain, O. Farkas, J. Tomasi, V. Barone, M. Cossi, R. Cammi, B. Mennucci, C. Pomelli, C. Adamo, S. Clifford, J. W. Ochterski, G. A. Petersson, P. Y. Ayala, Q. Cui, K. Morokuma, P. Salvador, J. J. Dannenberg, D. K. Malick, A. D. Rabuck, K. Raghavachari, J. B. Foresman, J. Cioslowski, J. V. Ortiz, A. G. Baboul, B. B. Stefanov, G. Liu, A. Liashenko, P. Piskorz, I. Komaromi, R. Gomperts, R. L. Martin, D. J. Fox, T. Keith, M. A. Al-Laham, C. Y. Peng, A. Nanayakkara, M. Challacombe, P. M. W. Gill, B. Johnson, W. Chen, M. W. Wong, J. L. Andres, C. Gonzalez, M. Head-Gordon, E. S. Replogle, J. A. Pople in *Gaussian 98*, Gaussian, Inc., Pittsburgh PA, **2001**.
[30] W. Kaim, *J. Am. Chem. Soc.* **1982**, *104*, 3833–3837.
[31] A. C. Bhasikuttan, M. Suzuki, S. Nakashima, T. Okada, *J. Am. Chem. Soc.* **2002**, *124*, 8398–8405.
[32] A. T. Yeh, C. V. Shank, J. K. McCusker, *Science* **2000**, *289*, 935–938.

[33] J. K. McCusker, *Acc. Chem. Res.* **2003**, *36*, 876–887.
[34] J. N. Demas, D. G. Taylor, *Inorg. Chem.* **1979**, *18*, 3177–3179.
[35] R. W. Harrigan, G. A. Crosby, *J. Chem. Phys.* **1973**, *59*, 3468–3476.
[36] C. Creutz, M. Chou, T. L. Netzel, M. Okumura, N. Sutin, *J. Am. Chem. Soc.* **1980**, *102*, 1309–1319.
[37] P. S. Braterman, A. Harriman, G. A. Heath, L. J. Yellowlees, *J. Chem. Soc. Dalton Trans.* **1983**, 1801–1803.
[38] O. Shimizu, J. Watanabe, S. Naito, *Chem. Phys. Lett.* **2000**, *332*, 295–298.
[39] N. H. Damrauer, J. K. McCusker, *J. Phys. Chem. A* **1999**, *103*, 8440–8446.
[40] A. E. Curtright, J. K. McCusker, *J. Phys. Chem. A* **1999**, *103*, 7032–7041.
[41] E. Krausz, *Com. Inorg. Chem.* **1988**, *7*, 139–158.
[42] M. K. Brennaman, J. H. Alstrum-Acevedo, C. N. Fleming, P. Jang, T. J. Meyer, J. M. Papanikolas, *J. Am. Chem. Soc.* **2002**, *124*, 15094–15098.
[43] R. J. Watts, *J. Chem. Educ.* **1983**, *60*, 834–842.
[44] A. Juris, V. Balzani, F. Barigelletti, S. Campagna, P. Belser, A. von Zelewsky, *Coord. Chem. Rev.* **1988**, *84*, 85–277.
[45] E. M. Kober, T. J. Meyer, *Inorg. Chem.* **1982**, *21*, 3967–3977.
[46] K. W. Hipps, G. A. Crosby, *J. Am. Chem. Soc.* **1975**, *97*, 7042–7048.
[47] G. A. Crosby, K. W. Hipps, W. H. Elfring, Jr., *J. Am. Chem. Soc.* **1974**, *96*, 629–630.
[48] E. M. Kober, T. J. Meyer, *Inorg. Chem.* **1984**, *23*, 3877–3886.
[49] G. A. Crosby, W. H. Elfring. Jr., *J. Phys. Chem.* **1976**, *80*, 2206–2211.
[50] D. Braun, P. Huber, J. Wudy, J. Schmidt, H. Yersin, *J. Phys. Chem.* **1994**, *98*, 8044–8049.
[51] P. G. Bradley, K. Nurit, B. A. Hornberger, R. F. Dallinger, W. H. Woodruff, *J. Am. Chem. Soc.* **1981**, *103*, 7441–7446.
[52] P. J. Carroll, L. E. Brus, *J. Am. Chem. Soc.* **1987**, *109*, 7613–7616.
[53] T. Yabe, L. K. Orman, D. R. Anderson, S.-C. Yu, X. Xu, J. B. Hopkins, *J. Phys. Chem.* **1990**, *94*, 7128–7132.

Received: April 29, 2005
Revised: August 24, 2005
Published online: November 3, 2005

